Applied Surface Science 577 (2022) 151976

Contents lists available at ScienceDirect

Applied Surface Science

journal homepage: www.elsevier.com/locate/apsusc

Full Length Article

Nanosecond pulsed laser-induced formation of nanopattern on Fe-based metallic glass surface

Yongfeng Qian [a], Hu Huang [a,*], Minqiang Jiang [b,c], Jiwang Yan [d]

[a] Key Laboratory of CNC Equipment Reliability, Ministry of Education, School of Mechanical and Aerospace Engineering, Jilin University, Changchun, Jilin, 130022, China
[b] State Key Laboratory of Nonlinear Mechanics, Institute of Mechanics, Chinese Academy of Sciences, Beijing 100190, China
[c] School of Engineering Science, University of Chinese Academy of Sciences, Beijing 100049, China
[d] Department of Mechanical Engineering, Faculty of Science and Technology, Keio University, Yokohama 223-8522, Japan

ARTICLE INFO

Keywords:
Metallic glass
Laser irradiation
Microstructure
Formation mechanism
Element enrichment

ABSTRACT

Fe-based metallic glasses (MGs) have attracted much attention because of their cheap raw materials, outstanding soft magnetic properties and superior catalytic activity. Meanwhile, the fabrication of micro/nano-structures on its surface could further improve its functional properties. In this study, it was attempted to fabricate micro/nano-structures on a Fe-based MG ($Fe_{52}Cr_{13}Mo_{12}C_{15}B_6Er_2$, in at. %) surface by nanosecond pulsed laser irradiation technology. The surface characteristics and microstructural evolution of Fe-based MG were investigated. The experimental results showed that under different laser fluences, the laser-irradiated areas exhibited distinguished microstructures, i.e., nanoparticles, the network nanostructures or a combination of these two microstructures. Furthermore, oxygen and erbium were enriched inside the network nanostructures. By analyzing the microstructural evolution, formation mechanisms of the nanoparticles and the network nanostructures were discussed. The nanoparticles were actually caused by laser-induced element enrichment (i.e. amorphous erbium oxide) and the mismatch of its wettability with the substrate; the formation of the network nanostructures was attributed to the diffusion and connection of nanoparticles under the combined influence of recoil pressure and surface topography.

1. Introduction

With a long-range disordered atomic structure [1,2], metallic glasses (MGs) exhibit many fascinating properties and functionalities, such as high hardness [3–6], high elastic energy [7,8], outstanding resistance to wear and corrosion [9,10] as well as excellent biocompatibility [11–15]. However, the size of MGs is relatively small due to the limitation of the critical cooling rate required during the preparation process [16], which has become a main obstacle in the practical engineering application of MGs. To overcome this problem, multicomponent rule was proposed and applied to prepare MGs with high glass forming ability (GFA) [17], typically including Pd- [18], Zr- [19,20], Ti- [21], and Fe-based MGs [22,23]. In particular, compared with other MGs, Fe-based MGs have been attracted more attention in engineering applications because of their cheap industrial raw materials [24] and outstanding soft magnetic properties [25,26]. Moreover, the superior catalytic activity of Fe-based MGs also inspired the exploration of chemical applications, including the wastewater and organic pollutant remediation [27,28], oxidative degradation [29] and so on. On the other hand, it has been confirmed that the fabrication of micro/nano-structures on the surface of materials could further improve the catalytic activity owing to the increase of effective surface area [30,31]. Furthermore, surface wettability [32,33] and biofunctionality [34,35] could also be changed by introducing micro/nano-structures on material surfaces. Therefore, the fabrication of micro/nano-structures with tailored properties on the MG surface has always fascinated researchers.

Typical processing technologies, including mechanical processing [36,37] and chemical corrosion [38,39], are widely used to fabricate micro/nano-structures on the surface of materials. However, these two methods may be not ideal for Fe-based MGs. Due to inherent hard-brittle features of Fe-based MGs, it is relatively difficult to generate surface micro/nano-structures by mechanical processing; at the same time, the wear of cutting tool will be quite serious because of its high hardness. For chemical corrosion, the choice of corrosion solution is very limited

* Corresponding author.
E-mail address: huanghu@jlu.edu.cn (H. Huang).

https://doi.org/10.1016/j.apsusc.2021.151976
Received 6 June 2021; Received in revised form 17 November 2021; Accepted 18 November 2021
Available online 20 November 2021

Table 1
Experimental conditions.

Sample material	$Fe_{52}Cr_{13}Mo_{12}C_{15}B_6Er_2$
Wavelength, nm	532
Pulse width, ns	15.4
Repetition frequency, kHz	1
Laser scanning speed, mm/s	1
Laser fluence, J/cm^2	0.85, 1.39, 1.89

because of the excellent corrosion resistance of Fe-based MGs. Thus, it is meaningful to develop some new methods for patterning the Fe-based MGs.

In recent years, laser irradiation technology has been gradually applied to pattern the MG surface by virtue of its non-contact and versatility. After laser irradiation, various surface micro/nano structures have been produced on the MGs surface, broadening their functional applications [32,40–43]. For example, by nanosecond pulsed laser processing, Jiao et al. successfully fabricated the dimple and groove structures on a Vit 105 Zr-based MG, thereby modifying its surface wettability [42]. By femtosecond laser irradiation, non-centrosymmetric surface structures were formed on a Zr-based MG surface, realizing the unidirectional water micro-diplacement [43]. However, the current studies on laser surface patterning of MGs are mainly focused on special types of MGs, i.e. Zr-based MG systems, and the investigations on the response of Fe-based MGs to nanosecond pulsed laser irradiation are relatively lacking.

Accordingly, in this study, a Fe-based MG was irradiated by a nanosecond pulsed laser at ambient environment. The effects of laser fluence on the surface morphology were systematically investigated. It was found that nanoparticles and network nanostructures could be induced on the Fe-based MG surface. Further, formation mechanisms of the nanoparticles and the network nanostructures were discussed.

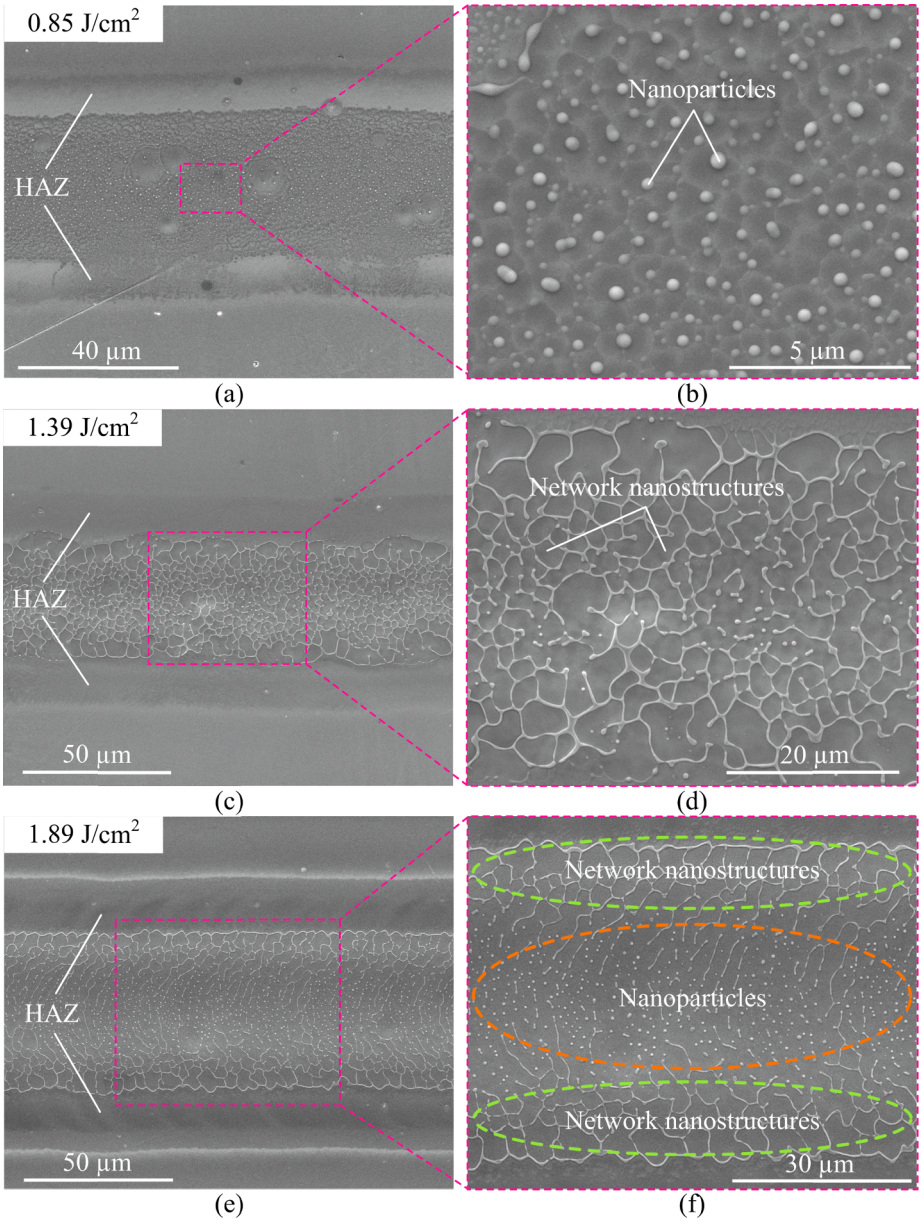

Fig. 1. SEM morphologies of the Fe-based MG surface after laser irradiation under various laser fluences: (a-b) 0.85 J/cm^2, (c-d) 1.39 J/cm^2, and (e-f) 1.89 J/cm^2.

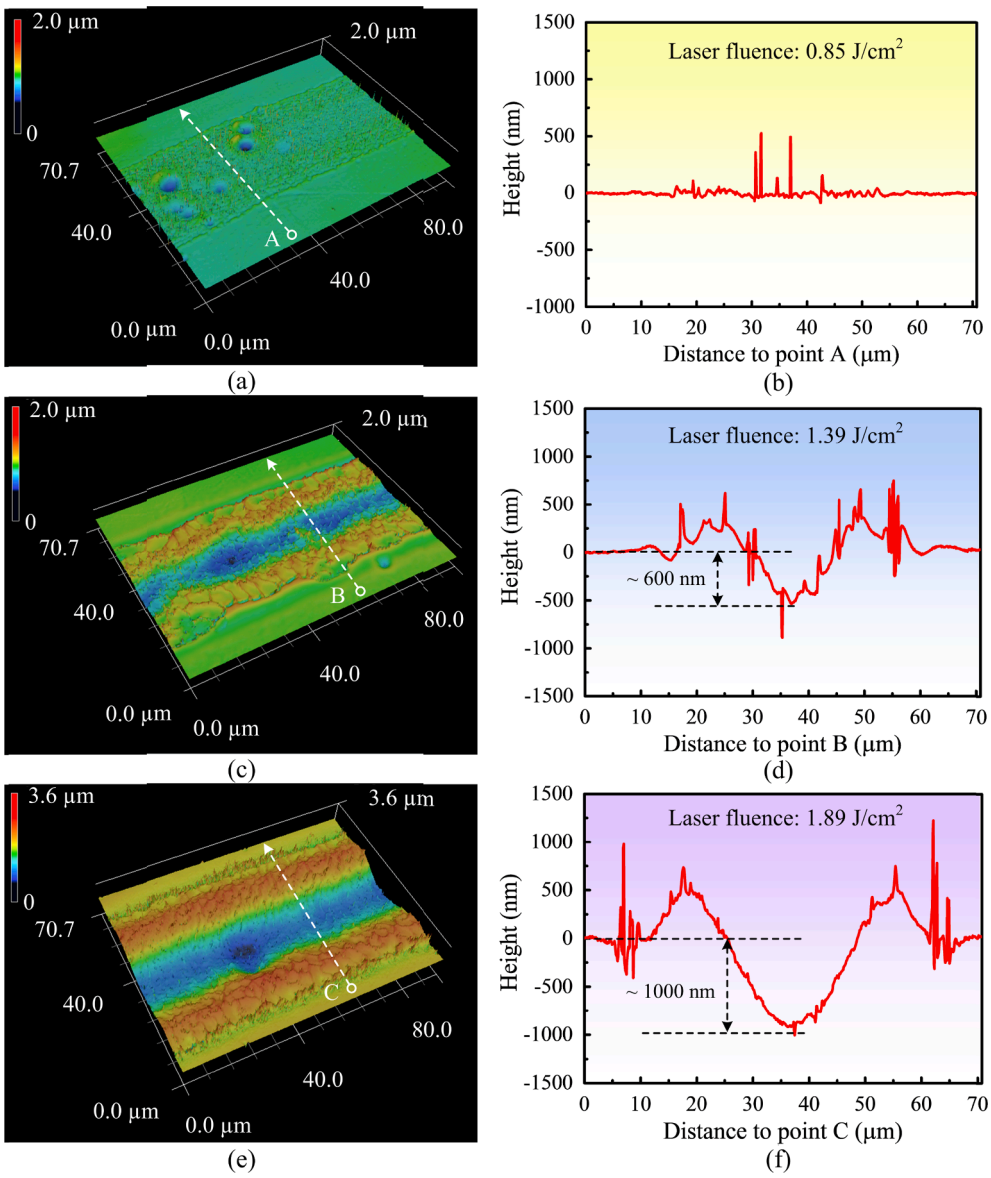

Fig. 2. 3D images and the corresponding height profiles of laser-irradiated Fe-based MG surfaces with different laser fluences: (a-b) 0.85 J/cm^2, (c-d) 1.39 J/cm^2, and (e-f) 1.89 J/cm^2.

2. Materials and methods

2.1. Materials

$Fe_{52}Cr_{13}Mo_{12}C_{15}B_6Er_2$ (in at. %) alloy ingots were first prepared by arc-melting the mixtures of pure constituent elements under argon atmosphere. The purities of the metals were 99.9 wt% for Fe, 99.99 wt% for Cr, 99.9 wt% for Mo, 99.99 wt% for C, 99.9 wt% for B and 99.9 wt% for Er. The alloy ingots were re-melted four times to improve compositional homogeneity. Using these alloy ingots, rod samples of 7 mm in diameter were made by water-chilled copper mold suction casting.

The Fe-based MG rod was attempted to cut into slices with a thickness of 2 mm by wire electrical discharge machining (wire-EDM). However, fracture occurred during the wire-EDM process because of the concentrated thermal process, and only small pieces were obtained, further demonstrating its hard-brittle feature and poor machinability. Our previous studies [44,45] indicated that wire-EDM would induce crystallization layer on the machined MG surface. To remove the crystallization layer and obtain mirror sample surface, mechanical grinding was performed on the obtained Fe-based MG samples using 400, 800, and 1500 grit sand papers in sequence, followed by polishing using diamond paste. The amorphous characteristic of the polished MG was characterized by an X-ray diffractometer (XRD, D8 Discover, Bruker, Germany).

2.2. Laser irradiation

A Nd:YAG nanosecond pulsed laser system (LR-SHG, MegaOpto Co., Ltd., Japan) was used to perform laser irradiation of the Fe-based MG surface at ambient environment. It has a wavelength of 532 nm, a pulse width of 15.4 ns, and a laser beam diameter of ~ 85 μm with an approximate Gaussian intensity profile. The repetition frequency and scanning speed were set to 1 kHz and 1 mm/s, respectively. Various average laser powers, 0.048, 0.079, 0.107 W (corresponding to the laser fluences of 0.85, 1.39, and 1.89 J/cm^2, respectively) were used for comparison. It should be mentioned that when the laser fluence was further increased, remarkable micro-cracks appeared in the irradiated regions because of the high thermal stress gradient as well as the inherent brittleness of Fe-based MG. Table 1 presents the experimental conditions mentioned above.

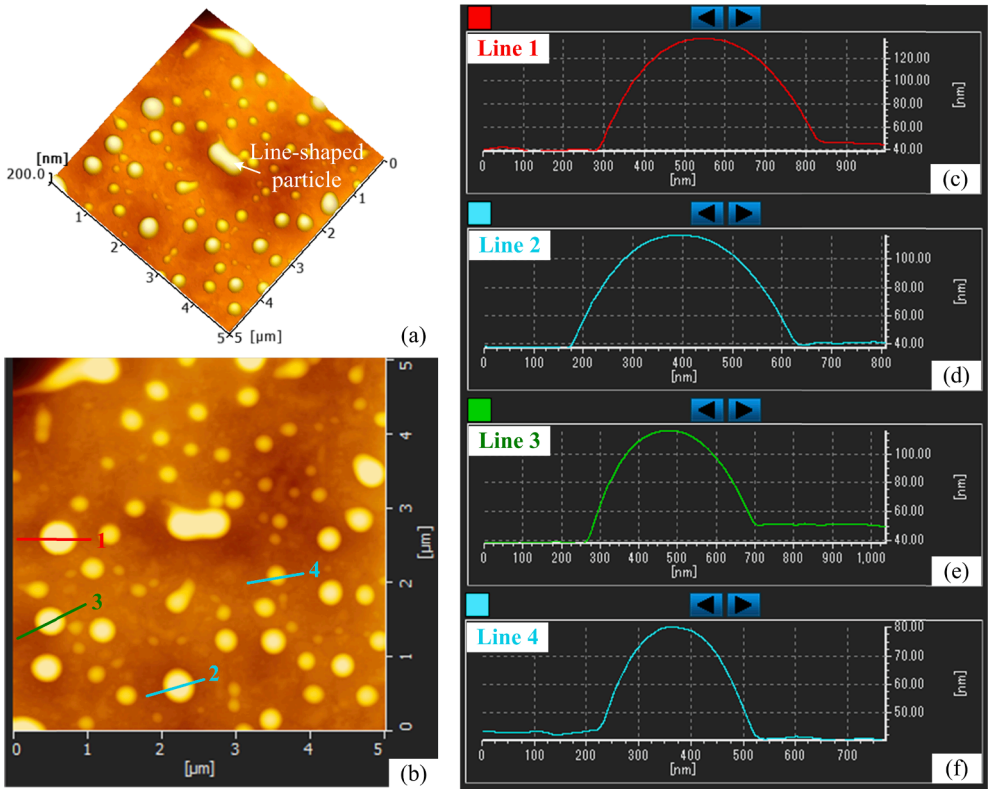

Fig. 3. The AFM images of the nanoparticles in Fig. 1(a): (a) 3D topography, (b) 2D topography, and (c)-(f) the height profiles of the Line 1- Line 4 in Fig. 3(b), respectively.

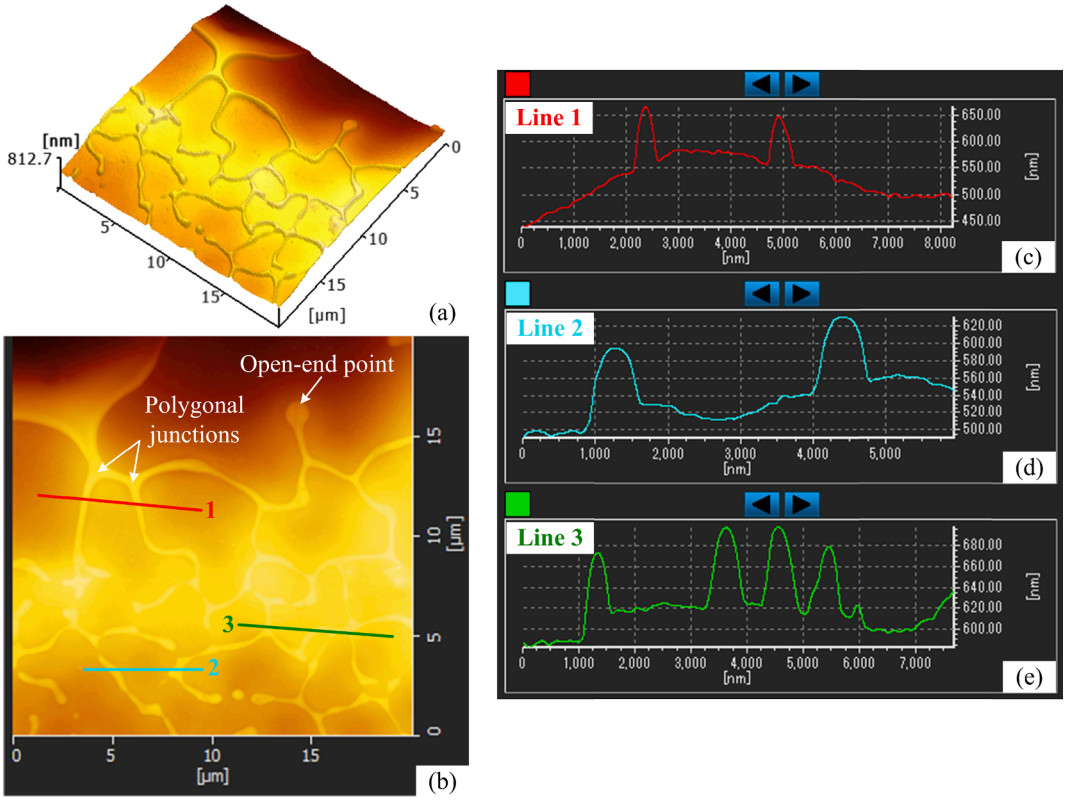

Fig. 4. The AFM images of the network nanostructures in Fig. 1(b): (a) 3D topography, (b) 2D topography, and (c)-(e) the height profiles of the Line 1- Line 3 in Fig. 4 (b), respectively.

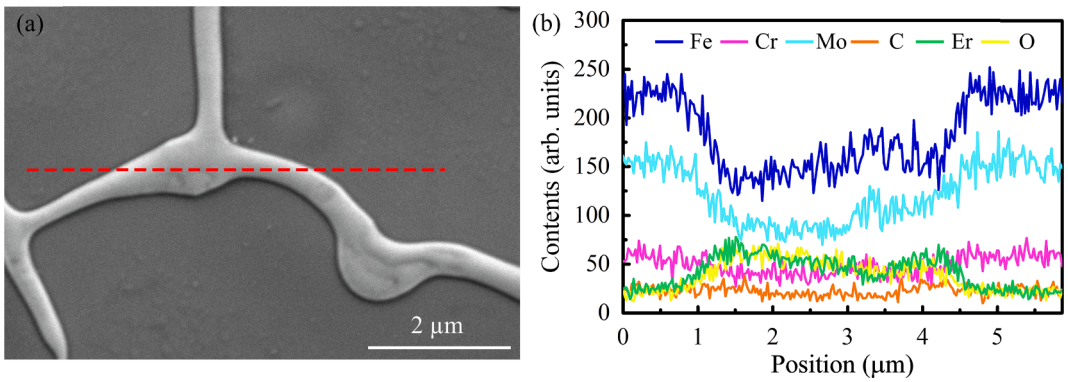

Fig. 5. (a) The position of SEM-EDS line measurement, and (b) the corresponding EDS line profiles along the marked line in Fig. 5(a).

2.3. Characterization

The laser-irradiated MG surfaces were observed by a field emission scanning electron microscope (FE-SEM, JSM-7600F, JEOL, Japan) and the surface topographies were further measured by a three-dimensional (3D) laser scanning microscope (VK-9700, Keyence, Japan) and an atomic force microscope (AFM, AFM 5100N, Hitachi, Japan). The element distribution in the irradiated regions was characterized by an energy dispersive X-ray spectroscopy (EDS, X-Max80, Oxford Instrument, UK). The cross-sectional characteristics of the surface microstructure were characterized by a transmission electron microscope (TEM, JEM-2100F, JEOL, Japan), and the TEM sample was prepared via a focused ion beam (FIB, S9000G, TESCAN, Czech).

3. Results and discussion

3.1. Microstructures

Fig. 1 presents the SEM morphologies of laser-irradiated Fe-based MG surface under various laser fluences. For a relatively low laser fluence (0.85 J/cm^2), a large number of discrete nanoparticles appear in the irradiated area, as seen in Figs. 1(a) and (b). When increasing the laser fluence to 1.39 J/cm^2, the irradiated area exhibits large-area network nanostructures, except for the HAZ (see Fig. 1(c)). It is noted that the network nanostructures are not always completely closed, especially in the center of the irradiated area. As the laser fluence further increases to 1.89 J/cm^2, the whole irradiated area is featured by two distinct microstructures, the network nanostructures around the HAZ and the nanoparticles located in the center of the irradiated area. In addition, from the surface morphologies in Figs. 1(a)-(f), it is assumed that the network nanostructures may be formed by the connection of nanoparticles.

In order to further observe the surface characteristics of laser-irradiated Fe-based MG, Figs. 2(a), (c) and (e) give the 3D images of laser-irradiated areas in Figs. 1(a), (c) and (e), respectively, and Figs. 2 (b), (d) and (f) give the height profiles along the marked lines in Figs. 2 (a), (c) and (e), respectively. In Figs. 2(a) and (b), there is no obvious height fluctuation in the entire irradiated area, which indicates that only shallow melting occurred under the relatively low laser fluence (0.85 J/cm^2). However, when the laser fluence increases to 1.39 J/cm^2 or more, the groove structures are generated on the MG surface. Furthermore, as the laser fluence increases, the depth of the groove structure will increase.

To capture more details on the nanoscale, the nanoparticles and network nanostructures were further characterized topographically by AFM. Figs. 3(a) and (b) present the details of the laser-irradiated area in Fig. 1(a) where many nanoparticles with big difference in size are visible. In addition, some nanoparticles are connected to each other, resulting in the formation of line-shaped particles. In Figs. 3(c)-(f), it can be seen that nanoparticles are about several hundred nanometers in diameter, and they behave as spherical droplets sitting on a flat surface. For the network nanostructures, the sizes of the polygonal junctions and the open-end points are relatively large (see Figs. 4(a) and (b)), which further indicates that they may originate from the connection of nanoparticles. In addition, as shown in Figs. 4(c)-(e), the dimensions of the network nanostructures are similar to those of nanoparticles, i.e., several hundred nanometers in diameter and less than 100 nm in height.

As seen in Fig. 1, compared to other areas, the nanoparticles and network nanostructures have brighter contrast, which suggests that the alloying element composition of the laser-irradiated area may be non-uniformed. As an example, the elements distribution across the network nanostructures was measured by EDS (see Fig. 5(a)), and the corresponding results are shown in Fig. 5(b). From Fig. 5(b), it can be qualitatively seen that the concentrations of Er and O elements in the

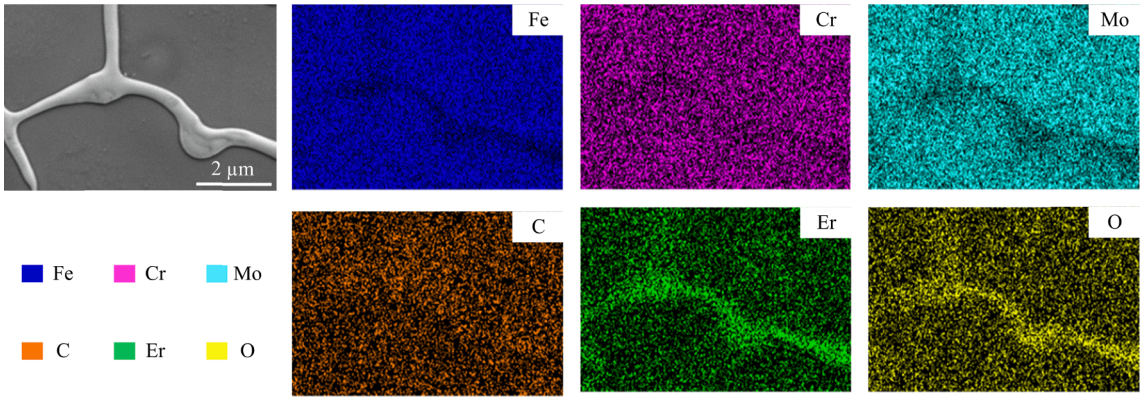

Fig. 6. SEM-EDS mapping results of the laser-irradiated area.

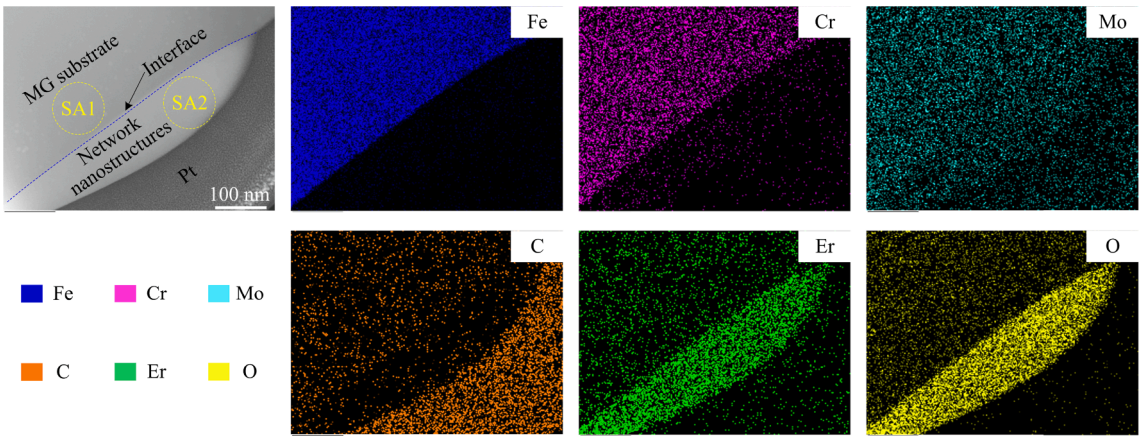

Fig. 7. TEM bright field image showing the interface between the MG substrate and the network nanostructures as well as its STEM-EDS mapping results.

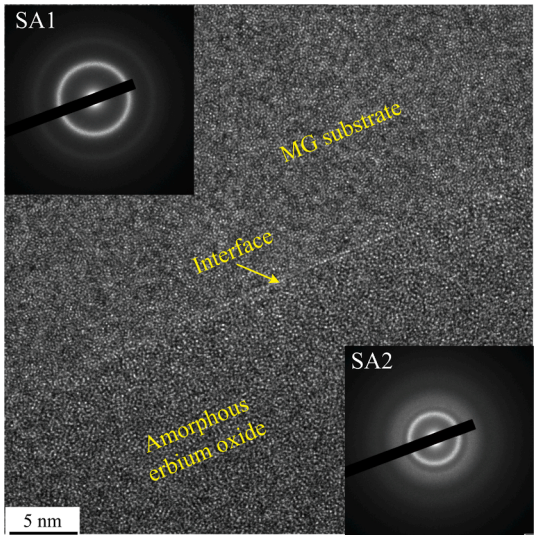

Fig. 8. HRTEM image showing the interface between the MG substrate and the network nanostructures. The insets show the selected area electron diffraction patterns taken from the MG substrate (SA1) and network nanostructures (SA2) in Fig. 7, respectively.

network nanostructures are significantly higher than those in other regions, while the other elements are just the opposite. This is further verified by the SEM-EDS mapping results shown in Fig. 6. It is noted that more Er and O elements are concentrated in the network nanostructures, and the other elements (Fe, Cr, Mo, C) are uniformly distributed. In Fig. 5(b) and Fig. 6, the distribution of oxygen and erbium elements is very consistent, suggesting that the nanoparticles and network nanostructures may be actually the erbium oxide.

To further confirm the chemical composition evolution induced by laser irradiation, a small cross-section involving the MG substrate and network nanostructures was extracted via FIB and then characterized by TEM. Fig. 7 presents the results. The STEM-EDS mapping results clearly reveal that the network nanostructures are mainly composed of Er and O elements, which are consistent with the SEM-EDS analysis results. Fig. 8 shows the high-resolution TEM (HRTEM) image at the interface. It is seen that both the MG substrate and the network nanostructures are fully amorphous. To further confirm this result, the selected area electron diffraction (SAED) were performed on the MG substrate (SA1) and network nanostructures (SA2) in Fig. 7, respectively, and the corresponding diffraction patterns are shown in the insets of Fig. 8. Regardless of the MG substrate or the network nanostructures, the diffraction pattern consists of only a halo ring, suggesting the amorphous characteristics of the newly formed network nanostructures (i.e. erbium oxide), which could be attributed to the fast heating and cooling processes during the laser irradiation.

3.2. Discussion on the surface microstructure formation and evolution

The above results indicate that under different laser fluences, the laser-irradiated surfaces exhibit different microstructures, i.e., nanoparticles, network nanostructures or a combination of these two microstructures. At the same time, since the network nanostructures are connected by adjacent nanoparticles, the formation mechanism of the nanoparticles should be investigated first. Fig. 9(a) presents a schematic diagram for illustrating the possible formation process of the nanoparticles. During the laser irradiation, the surface layer of the MG material would be heated and the surface temperature would rise sharply. At high temperature, the Er element contained in the sample would chemically react with the O element in the atmosphere, resulting in the formation of erbium oxide. In this case, due to the difference in chemical composition, the erbium oxides would be poorly wetted with other molten materials, so after solidification, they behave as spherical droplets sitting on the MG substrate, as shown in Fig. 9(a).

Next, the effects of laser fluence on the surface microstructures of laser-irradiated area will be discussed, and Fig. 9(b) presents the corresponding schematic diagram. In fact, due to the relatively small size of the nanoparticles, they are extremely unstable during the solidification process, and their movement would be affected by both forces and solid boundaries. For example, the recoil pressure, as a universal force in the laser-material interaction, will significantly affect the melt flow in the molten pool and further determine the surface topography of the laser-irradiated area. In turn, the existence of recoil pressure is generally confirmed by observing the surface topography of the laser-irradiated area. Especially, the formation of the groove structure is the most direct evidence to confirm the existence of recoil pressure. As shown in Figs. 2(a) and (b), at a relatively low laser fluence of 0.85 J/cm^2, the whole irradiated area exhibits a flat topography except for the nanoparticles, indicating that only shallow melting occurs on the MG surface under this laser fluence. Without the effect of recoil pressure, the alloy melts were relatively stable. Therefore, the nanoparticles would remain in their initial formation position rather than diffusion or connection. When the laser fluence is increased to 1.39 J/cm^2, the grooves with pileups around are formed on the MG surface as shown in Figs. 2(c)-(f), suggesting the existence of strong recoil pressure. Accordingly, under the effect of recoil pressure, the nanoparticles located in the center of the scanning line have a tendency to diffuse to both sides, leading to the interconnection of adjacent nanoparticles to form network nanostructures. Since the solidification starts from both sides to the center [46], the network nanostructures will firstly be formed on both sides of

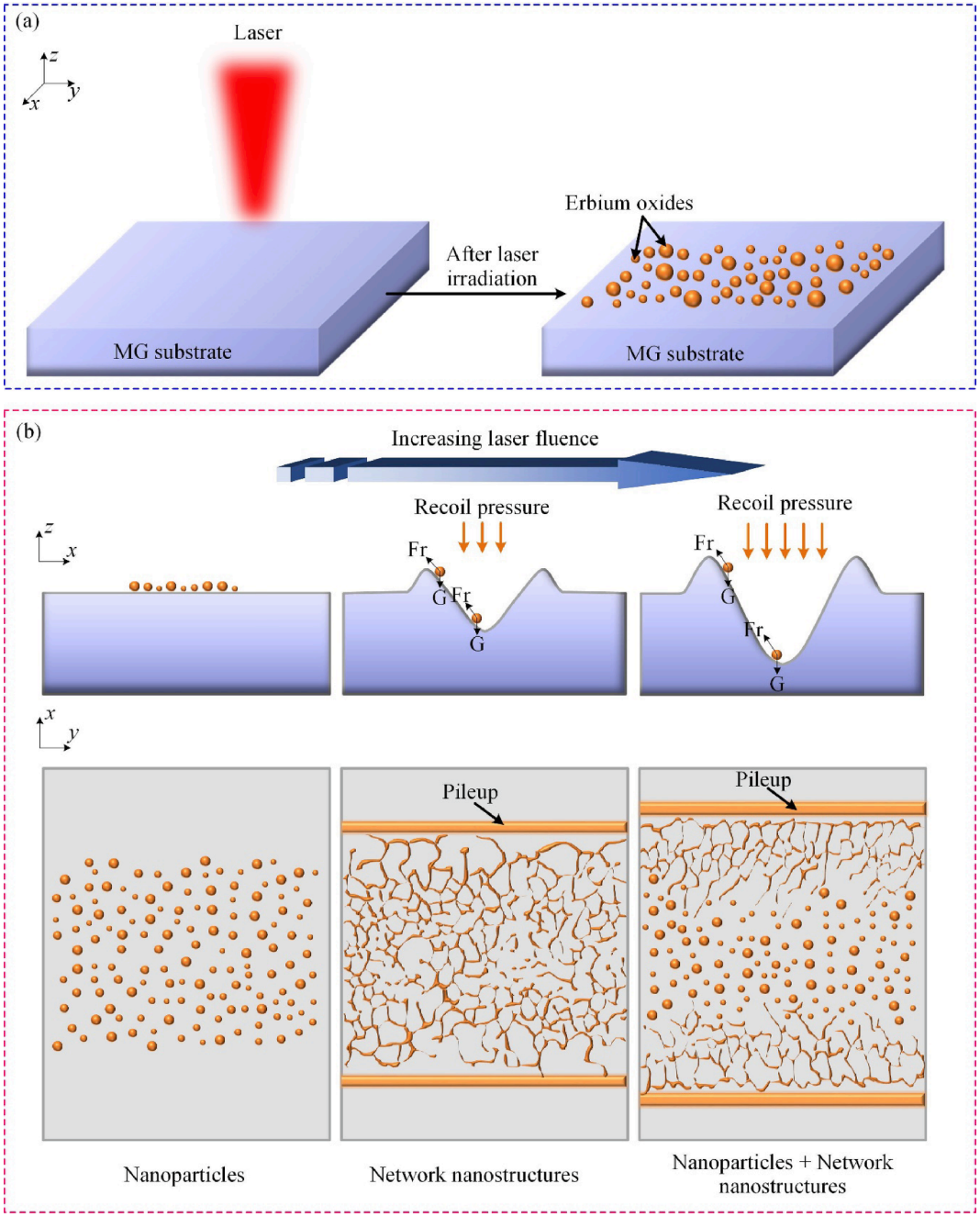

Fig. 9. (a) Schematic formation process of the nanoparticles on the Fe-based MG substrate. (b) The schematic diagram illustrating the effects of laser fluence on the surface microstructures of laser-irradiated area.

the scanning line. At the same time, the high pileups might act as the solid boundary that provides potential nucleation positions for the network nanostructures. When the laser fluence is further increased to 1.89 J/cm^2, more heat is delivered to the MG surface, resulting in an increase in the recoil pressure and the depth of the grooves. The larger recoil pressure will promote the movement of nanoparticles, and the network nanostructures would still form around the pileups. However, due to the relatively large depth of the grooves, the nanoparticles located at the bottom of the groove structure cannot overcome their own gravity to move sideways, thus remaining separate distribution without forming network nanostructures. The above results indicate that under these laser fluences, the formation of nanoparticles as well as their diffusion and connection determine the final surface microstructure.

4. Conclusions

In summary, the surface characteristics and microstructural evolution of $Fe_{52}Cr_{13}Mo_{12}C_{15}B_6Er_{22}$ MG under nanosecond pulsed laser irradiation were systematically investigated. The results showed that when increasing the laser fluence, the surface microstructures varied from nanoparticles to the network nanostructures, and then to a combination of these two microstructures. According to the EDS results, it was found that the network nanostructures were characterized by high oxygen and erbium enrichment. By analyzing the microstructural evolution, the formation mechanisms of the nanoparticles and the network nanostructures were discussed. The nanoparticles could be attributed to laser-induced element enrichment (i.e. amorphous erbium oxide) and the mismatch of its wettability with the substrate. In addition, the

diffusion and connection of nanoparticles under the combined influence of recoil pressure and surface topography would lead to the formation of network nanostructures. This study would not only enhance the fundamental understanding of laser-MG interaction, but also provides an effective approach for patterning Fe-based MG, which can improve their application potentials as functional materials.

CRediT authorship contribution statement

Yongfeng Qian: Investigation, Formal analysis, Data curation, Writing – original draft. **Hu Huang:** Conceptualization, Data curation, Funding acquisition, Methodology, Resources, Supervision, Writing – review & editing. **Minqiang Jiang:** Investigation, Methodology, Writing – review & editing. **Jiwang Yan:** Resources, Supervision.

Declaration of Competing Interest

The authors declare that they have no known competing financial interests or personal relationships that could have appeared to influence the work reported in this paper.

Acknowledgements

The authors would thank Dr. Jiliang Zhang for providing the Fe-based metallic glass. This work was supported by the National Natural Science Foundation of China (Grant No. 51705197), the Young Elite Scientists Sponsorship Program by CAST (YESS) (Grant No. 2017QNRC001), the Graduate Innovation Fund of Jilin University (Grant No. 101832020CX106), and the Fundamental Research Funds for the Central Universities (2019-2021).

References

[1] A. Hirata, P. Guan, T. Fujita, Y. Hirotsu, A. Inoue, A.R. Yavari, T. Sakurai, M. Chen, Direct observation of local atomic order in a metallic glass, Nat. Mater. 10 (1) (2011) 28–33, https://doi.org/10.1038/nmat2897.

[2] A. Hirata, L.J. Kang, T. Fujita, B. Klumov, K. Matsue, M. Kotani, A.R. Yavari, M. W. Chen, Geometric frustration of icosahedron in metallic glasses, Science 341 (6144) (2013) 376–379, https://doi.org/10.1126/science:1232450.

[3] M.M. Trexler, N.N. Thadhani, Mechanical properties of bulk metallic glasses, Prog. Mater. Sci. 55 (8) (2010) 759–839, https://doi.org/10.1016/j.pmatsci.2010.04.002.

[4] U. Ramamurty, S. Jana, Y. Kawamura, K. Chattopadhyay, Hardness and plastic deformation in a bulk metallic glass, Acta Mater. 53 (3) (2005) 705–717, https://doi.org/10.1016/j.actamat.2004.10.023.

[5] D.V. Louzguine-Luzgin, A.S. Trifonov, Y.P. Ivanov, A.K.A. Lu, A.V. Lubenchenko, A. L. Greer, Shear-induced chemical segregation in a Fe-based bulk metallic glass at room temperature, Sci. Rep. 11 (2021) 13650, https://doi.org/10.1038/s41598-021-92907-4.

[6] D.C. Hofmann, L.M. Andersen, J. Kolodziejska, S.N. Roberts, J.-P. Borgonia, W. L. Johnson, K.S. Vecchio, A. Kennett, Optimizing bulk metallic glasses for robust, highly wear-resistant Gears, Adv. Eng. Mater. 19 (1) (2017) 1600541, https://doi.org/10.1002/adem.v19.110.1002/adem.201600541.

[7] W. Liu, Q. Zeng, Q. Jiang, L. Wang, B. Li, Density and elasticity of $Zr_{46}Cu_{37.6}Ag_{8.4}Al_8$ bulk metallic glass at high pressure, Scripta Mater. 65 (6) (2011) 497–500, https://doi.org/10.1016/j.scriptamat.2011.06.006.

[8] W.H. Wang, Bulk metallic glasses with functional physical properties, Adv. Mater. 21 (45) (2009) 4524–4544, https://doi.org/10.1002/adma.v21:4510.1002/adma.200901053.

[9] D.D. Coimbrão, G. Zepon, G.Y. Koga, D.A. Godoy Pérez, F.H. Paes de Almeida, V. Roche, J.-C. Lepretre, A.M. Jorge Jr, C.S. Kiminami, C. Bolfarini, A. Inoue, W.J. Botta, Corrosion properties of amorphous, partially, and fully crystallized $Fe_{68}Cr_8Mo_4Nb_4B_{16}$ alloy, J. Alloy. Compd. 826 (2020) 154123, https://doi.org/10.1016/j.jallcom.2020.154123.

[10] G.Y. Koga, D. Travessa, G. Zepon, D.D. Coimbrão, A.M. Jorge, J.E. Berger, V. Roche, J.-C. Lepretre, C. Bolfarini, C.S. Kiminami, F. Wang, S.L. Zhu, A. Inoue, W.J. Botta, Corrosion resistance of pseudo-high entropy Fe-containing amorphous alloys in chloride-rich media, J. Alloy. Compd. 884 (2021) 161090, https://doi.org/10.1016/j.jallcom.2021.161090.

[11] T.H. Li, P.C. Wong, S.F. Chang, P.H. Tsai, J.S.C. Jang, J.C. Huang, Biocompatibility study on Ni-free Ti-based and Zr-based bulk metallic glasses, Mater. Sci. Eng. C 75 (2017) 1–6, https://doi.org/10.1016/j.msec.2017.02.006.

[12] M.S. Dambatta, S. Izman, B. Yahaya, J.Y. Lim, D. Kurniawan, Mg-based bulk metallic glasses for biodegradable implant materials: A review on glass forming ability, mechanical properties, and biocompatibility, J. Non-Cryst. Solids 426 (2015) 110–115, https://doi.org/10.1016/j.jnoncrysol.2015.07.018.

[13] B.-S. Lou, Y.-C. Yang, J.-W. Lee, L.-T. Chen, Biocompatibility and mechanical property evaluation of Zr-Ti-Fe based ternary thin film metallic glasses, Surf. Coat. Technol. 320 (2017) 512–519, https://doi.org/10.1016/j.surfcoat.2016.11.039.

[14] Y. Jiao, E. Brousseau, W. Nishio Ayre, E. Gait-Carr, X. Shen, X. Wang, S. Bigot, H. Zhu, W. He, In vitro cytocompatibility of a Zr-based metallic glass modified by laser surface texturing for potential implant applications, Appl. Surf. Sci. 547 (2021) 149194, https://doi.org/10.1016/j.apsusc.2021.149194.

[15] J.J. Lai, Y.S. Lin, C.H. Chang, T.Y. Wei, J.C. Huang, Z.X. Liao, C.H. Lin, C.H. Chen, Promising Ta-Ti-Zr-Si metallic glass coating without cytotoxic elements for bio-implant applications, Appl. Surf. Sci. 427 (2018) 485–495, https://doi.org/10.1016/j.apsusc.2017.08.065.

[16] W.L. Johnson, J.H. Na, M.D. Demetriou, Quantifying the origin of metallic glass formation, Nat. Commun. 7 (2016) 10313, https://doi.org/10.1038/ncomms10313.

[17] A. Inoue, High strength bulk amorphous alloys with low critical cooling rates, Mater. Trans. 36 (1995) 866–875, https://doi.org/10.2320/matertrans1989.36.866.

[18] W. Zhang, H. Guo, Y.H. Li, Y.M. Wang, H. Wang, M.W. Chen, S. Yamaura, Formation and properties of P-free Pd-based metallic glasses with high glass-forming ability, J. Alloy. Compd. 617 (2014) 310–313, https://doi.org/10.1016/j.jallcom.2014.07.214.

[19] Q.S. Zhang, W. Zhang, A. Inoue, Ni-free Zr–Fe–Al–Cu bulk metallic glasses with high glass-forming ability, Scripta Mater. 61 (3) (2009) 241–244, https://doi.org/10.1016/j.scriptamat.2009.03.056.

[20] Y. Zhang, D.Q. Zhao, M.X. Pan, W.H. Wang, Glass forming properties of Zr-based bulk metallic alloys, J. Non-Cryst. Solids 315 (2003) 206–210. 10.1016/S0022-3093(02)01876-8.

[21] K.-F. Xie, K.-F. Yao, T.-Y. Huang, A Ti-based bulk glassy alloy with high strength and good glass forming ability, Intermetallics 18 (10) (2010) 1837–1841, https://doi.org/10.1016/j.intermet.2010.02.036.

[22] Z.Y. Chang, X.M. Huang, L.Y. Chen, M.Y. Ge, Q.K. Jiang, X.P. Nie, J.Z. Jiang, Catching Fe-based bulk metallic glass with combination of high glass forming ability, ultrahigh strength and good plasticity in Fe–Co–Nb–B system, Mater. Sci. Eng. A 517 (1-2) (2009) 246–248, https://doi.org/10.1016/j.msea.2009.03.082.

[23] J. Shen, Q. Chen, J. Sun, H. Fan, G. Wang, Exceptionally high glass-forming ability of an FeCoCrMoCBY alloy, Appl. Phys. Lett. 86 (15) (2005) 151907, https://doi.org/10.1063/1.1897426.

[24] H.X. Li, Z.C. Lu, S.L. Wang, Y. Wu, Z.P. Lu, Fe-based bulk metallic glasses: Glass formation, fabrication, properties and applications, Prog. Mater. Sci. 103 (2019) 235–318, https://doi.org/10.1016/j.pmatsci.2019.01.003.

[25] M. Xu, Q.J. Wang, Fe-based bulk metallic glass with good soft magnetic properties, Mater. Sci. Forum 789 (2014) 59–63, https://doi.org/10.4028/www.scientific.net/MSF.789.59.

[26] F. Wang, A. Inoue, F.L. Kong, S.L. Zhu, E. Shalaan, F. Al-Marzouki, W.J. Botta, C. S. Kiminami, Y.P. Ivanov, A.L. Greer, Formation, stability and ultrahigh strength of novel nanostructured alloys by partial crystallization of high-entropy $(Fe_{0.25}Co_{0.25}Ni_{0.25}Cr_{0.125}Mo_{0.125})_{86-89}B_{11-14}$ amorphous phase, Acta Mater. 170 (2019) 50–61, https://doi.org/10.1016/j.actamat.2019.03.019.

[27] J.-Q. Wang, Y.-H. Liu, M.-W. Chen, G.-Q. Xie, D.V. Louzguine-Luzgin, A. Inoue, J. H. Perepezko, Rapid degradation of azo dye by Fe-based metallic glass powder, Adv. Funct. Mater. 22 (12) (2012) 2567–2570, https://doi.org/10.1002/adfm.201103015.

[28] H. Sun, H. Zheng, X. Yang, Efficient degradation of orange II dye using Fe-based metallic glass powders prepared by commercial raw materials, Intermetallics 129 (2021) 107030, https://doi.org/10.1016/j.intermet.2020.107030.

[29] L.-C. Zhang, S.-X. Liang, Fe-based metallic glasses in functional catalytic applications, Chem. Asian J. 13 (23) (2018) 3575–3592, https://doi.org/10.1002/asia.v13.2310.1002/asia.201801082.

[30] N. Chen, R. Frank, N. Asao, D.V. Louzguine-Luzgin, P. Sharma, J.Q. Wang, G. Q. Xie, Y. Ishikawa, N. Hatakeyama, Y.C. Lin, M. Esashi, Y. Yamamoto, A. Inoue, Formation and properties of Au-based nanograined metallic glasses, Acta Mater. 59 (16) (2011) 6433–6440, https://doi.org/10.1016/j.actamat.2011.07.007.

[31] M. Zhao, K. Abe, S.-I. Yamaura, Y. Yamamoto, N. Asao, Fabrication of Pd–Ni–P metallic glass nanoparticles and their application as highly durable catalysts in methanol electro-oxidation, Chem. Mater. 26 (2) (2014) 1056–1061, https://doi.org/10.1021/cm403185h.

[32] H. Huang, J. Yan, Surface patterning of Zr-based metallic glass by laser irradiation induced selective thermoplastic extrusion in nitrogen gas, J. Micromech. Microeng. 27 (7) (2017) 075007, https://doi.org/10.1088/1361-6439/aa71d5.

[33] M. Hasan, J. Warzywoda, G. Kumar, Decoupling the effects of surface texture and chemistry on the wetting of metallic glasses, Appl. Surf. Sci. 447 (2018) 355–362, https://doi.org/10.1016/j.apsusc.2018.03.205.

[34] A. Cunha, A.-M. Elie, L. Plawinski, A.P. Serro, A.M. Botelho do Rego, A. Almeida, M.C. Urdaci, M.-C. Durrieu, R. Vilar, Femtosecond laser surface texturing of titanium as a method to reduce the adhesion of *Staphylococcus aureus* and *biofilm formation*, Appl. Surf. Sci. 360 (2016) 485–493, https://doi.org/10.1016/j.apsusc.2015.10.102.

[35] A. Carvalho, L. Cangueiro, V. Oliveira, R. Vilar, M.H. Fernandes, F.J. Monteiro, Femtosecond laser microstructured Alumina toughened Zirconia: A new strategy to improve osteogenic differentiation of hMSCs, Appl. Surf. Sci. 435 (2018) 1237–1245, https://doi.org/10.1016/j.apsusc.2017.11.206.

[36] S.J. Zhang, Y.P. Zhou, H.J. Zhang, Z.W. Xiong, S. To, Advances in ultra-precision machining of micro-structured functional surfaces and their typical applications, Inter. J. Mach. Tool. Manuf. 142 (2019) 16–41, https://doi.org/10.1016/j.ijmachtools.2019.04.009.

[37] Z. Zhu, L.i. Chen, P. Huang, L. Schonemann, O. Riemer, J. Yao, S. To, W.-L. Zhu, Design and control of a piezoelectrically actuated fast tool servo for diamond turning of microstructured surfaces, IEEE Trans. Ind. Electron. 67 (8) (2020) 6688–6697, https://doi.org/10.1109/TIE.4110.1109/TIE.2019.2937051.

[38] H.Y. Zhang, J. Fornell, Y.P. Feng, I. Golvano, M.D. Baró, E. Pellicer, J. Sort, Inducing surface nanoporosity on Fe-based metallic glass matrix composites by selective dealloying, Mater. Charact. 153 (2019) 46-51, https:// doi.org/10.1016/j.matchar.2019.04.025.

[39] Lei Zuo, Ran Li, Yu Jin, Hongjie Xu, Tao Zhang, Fabrication of three-dimensional nanoporous nickel by dealloying Mg-Ni-Y metallic glasses in citric acid solutions for high-performance energy storage, J. Electrochem. Soc. 164 (2) (2017) A348–A354, https://doi.org/10.1149/2.1131702jes.

[40] H. Huang, N. Jun, M.Q. Jiang, M. Ryoko, J.W. Yan, Nanosecond pulsed laser irradiation induced hierarchical micro/nanostructures on Zr-based metallic glass substrate, Mater. Des. 109 (2016) 153–161, https://doi.org/10.1016/j.matdes.2016.07.056.

[41] R. Yamada, N. Nomura, J.J. Saida, A. Kawasaki, Fabrication of optical gratings through surface patterning of zirconium-based metallic glass by laser irradiation, Intermetallics 93 (2018) 377–382, https://doi.org/10.1016/j.intermet.2017.11.003.

[42] Yang Jiao, Emmanuel Brousseau, Xiaojun Shen, Xiaoxiang Wang, Quanquan Han, Hanxing Zhu, Samuel Bigot, Weifeng He, Investigations in the fabrication of surface patterns for wettability modification on a Zr-based bulk metallic glass by nanosecond laser surface texturing, J. Mater. Process. Technol. 283 (2020) 116714, https://doi.org/10.1016/j.jmatprotec.2020.116714.

[43] Chen Li, Lijun Yang, Xuezhuang Ren, Yong Yang, Guanghua Cheng, Femtosecond laser-induced non-centrosymmetric surface microstructures on bulk metallic glass for unidirectional droplet micro-displacement, J. Phys. D: Appl. Phys. 53 (10) (2020) 105305, https://doi.org/10.1088/1361-6463/ab5df7.

[44] H. Huang, J.W. Yan, Microstructural changes of Zr-based metallic glass during micro-electrical discharge machining and grinding by a sintered diamond tool, J. Alloy. Compd. 688 (2016) 14-21, https://dx. doi.org/10.1016/j.jallcom.2016.07.181.

[45] H. Huang, J.W. Yan, On the surface characteristics of a Zr-based bulk metallic glass processed by microelectrical discharge machining, Appli Surf. Sci. 355 (2015) 1306–1315, https://doi.org/10.1016/j.apsusc.2015.08.239.

[46] H Huang, Y.F Qian, C Wang, J.W Yan, Laser induced micro-cracking of Zr-based metallic glass using 10^{11} W/m^2 nano-pulses, Mater. Today Commun. 25 (2020) 101554, https://doi.org/10.1016/j.mtcomm.2020.101554.